EEG Gamma Band Oscillations Differentiate the Planning of Spatially Directed Movements of the Arm Versus Eye: Multivariate Empirical Mode Decomposition Analysis

Cheolsoo Park, Markus Plank, Joseph Snider, Sanggyun Kim, *Member, IEEE*, He Crane Huang, Sergei Gepshtein, Todd P. Coleman, and Howard Poizner

***Abstract*—The neural dynamics underlying the coordination of spatially-directed limb and eye movements in humans is not well understood. Part of the difficulty has been a lack of signal processing tools suitable for the analysis of nonstationary electroencephalographic (EEG) signals. Here, we use multivariate empirical mode decomposition (MEMD), a data-driven approach that does not employ predefined basis functions. High-density EEG, and arm and eye movements were synchronously recorded in 10 subjects performing time-constrained reaching and/or eye movements. Subjects were allowed to move both the hand and the eyes, only the hand, or only the eyes following a 500–700 ms delay interval where the hand and gaze remained on a central fixation cross. An additional condition involved a nonspatially-directed "lift" movement of the hand. The neural activity during a 500 ms delay interval was decomposed into intrinsic mode functions (IMFs) using MEMD. Classification analysis revealed that gamma band (30 Hz $<$) IMFs produced more classifiable features differentiating the EEG according to the different upcoming movements. A benchmark test using conventional algorithms demonstrated that MEMD was the best algorithm for extracting oscillatory bands from EEG, yielding the best classification of the different movement conditions. The gamma rhythm decomposed using MEMD showed a higher correlation with the eventual movement accuracy than any other band rhythm and than any other algorithm.**

Manuscript received November 13, 2013; revised March 26, 2014; accepted May 25, 2014. Date of publication June 30, 2014; date of current version September 04, 2014. The present research has been supported in part by the National Science Foundation (NSF) under Grant SMA-1041755 and Grant ENG-1137279 (EFRI M3C), in part by the Office of Naval Research (ONR) Multidisciplinary University Initiative (MURI) under Award N00014-10-1-0072, and in part by the Research Grant of Kwangwoon University in 2014.

C. Park is with the Department of Computer Engineering, Kwangwoon University, Seoul 139-701, Korea (e-mail: parkcheolsoo@kw.ac.kr).

M. Plank is with Brain Products GmbH, 82205 Gilching, Germany (e-mail: markusplank79@gmail.com).

J. Snider and H. Poizner are with the Institute for Neural Computation, University of California-San Diego, La Jolla, CA 92093 USA (e-mail: oldstyle_joe@yahoo.com; hpoizner@yahoo.com).

S. Kim and T. P. Coleman are with the Department of Bioengineering, University of California-San Diego, La Jolla, CA 92093 USA (e-mail: s2kim@ucsd.edu; tpcoleman@ucsd.edu).

H. C. Huang is with the Department of Cognitive Science, University of California-San Diego, La Jolla, CA 92093 USA (e-mail: crane081@gmail.com).

S. Gepshtein is with Center for Neurobiology of Vision, The Salk Institute for Biological Studies, La Jolla, CA 92037 USA (e-mail: sergei@salk.edu).

Digital Object Identifier 10.1109/TNSRE.2014.2332450

***Index Terms*—Electroencephalographic (EEG), empirical mode decomposition, motor control, reaching control, NA-MEMD.**

I. Introduction

PLANNING the movements of the eyes and hands involves transformations of spatial representations of arms, eyes, and the target [1]. The planning of saccades and hand movements is partially mediated by the bidirectional neural networks linking the parietal and frontal areas of the cortex [2]. The neural dynamics underlying such planning in humans is poorly understood. The noninvasive electroencephalography (EEG) and magnetoencephalography (MEG) have been increasingly used to investigate the temporal dynamics of sensorimotor and cognitive processes. For example, Perfetti *et al.* [3] recorded EEG while healthy subjects learned a visuo-motor rotation task, and found that gamma and theta activity were modulated during movement planning and execution. Initial learning was associated with increasing gamma power over the right parietal cortices during execution of reaching movements, and with gamma/theta phase coherence during movement planning. Werf *et al.* [4], [5] used MEG to demonstrate neuronal synchronization of gamma band activity in the human posterior parietal cortex during both reaching movements and saccade planning.

Previous studies of neuronal oscillations in different frequency bands during reaching movements have tended to employ standard signal processing techniques based on Fourier analysis and wavelet analysis [3]–[6]. These methods use predefined sets of basis functions resulting in poor time-frequency localization [7]. The fixed linear basis functions that are effective for stationary modeling can be sub-optimal for the nonstationary electrophysiological signals of the brain [8]–[10]. In such biological systems as the brain the frequencies of oscillations are not fixed: EEG rhythms drift within different frequency bands, making the conventional methods based on predefined bases inadequate. In the present work, we take into account the nonstationary and nonlinear neuronal oscillations by using empirical mode decomposition (EMD) [7], which is a fully data-driven time-frequency analysis algorithm. EMD makes no prior assumptions about the data, which makes it highly suitable

for the analysis of intracortical signals and EEG [9], [11]–[13]. For example, Park *et al.* demonstrated a better localization of time-varying frequency components of mu and $beta$ rhythms during motor imagery using the EMD algorithm, crossing over the fixed frequency bands, than such conventional methods as short-time Fourier transform (STFT) and wavelet transform [8].

Furthermore, the analysis of multichannel EEG on a channel-by-channel basis does not consider cross-channel interdependence. Fourier and wavelet transforms decompose the signal from each EEG channel separately by applying fixed basis functions. The original EMD algorithm was also designed for single-channel data decomposition without consideration of cross-channel interdependence, posing a problem of uniqueness: the phenomenon where the components for each channel do not correspond in number and frequency [14]. Recently developed multivariate empirical mode decomposition (MEMD) can be used to circumvent the problem of uniqueness and yield a more accurate estimation of the intrinsic modes in multichannel signals when narrowband oscillations of interest are shared by multiple channels [15].

This paper presents the analysis of EEG during the planning of spatially (or nonspatially) directed reaching movements and saccade movements using MEMD with a support vector machine (SVM)[1] classification tool [18]. We discriminate time-frequency components of single trials using MEMD as well as Fourier and wavelet transforms in different tasks, and investigate which method extracts features of cortical signals more accurately to represent the different conditions.

II. Methods

A. Empirical Mode Decomposition

Empirical mode decomposition (EMD) makes no prior assumptions on the data which makes it suitable for the analysis of nonlinear and nonstationary processes [7]. EMD is a fully data-driven technique for decomposing the signal into amplitude modulation (AM) and frequency modulation (FM) components, known as intrinsic mode functions (IMF), which reflects the natural oscillations of the signal. A signal requires two conditions to be considered an IMF: 1) the number of extrema and the number of zero crossings differ at most by one, 2) the mean of the envelopes connecting the local maxima and local minima is approximately zero. The steps of EMD decomposition are outlined in Algorithm 1.

Algorithm 1. The standard EMD algorithm

0) Input signal, $v(t)$.
1) Let $\tilde{v}(t) = v(t)$.
2) Identify all local maxima and minima of $\tilde{v}(t)$.
3) Find a lower "envelope," $e_l(t)$ that interpolates all local minima.
4) Find an upper "envelope," $e_u(t)$ that interpolates all local maxima.
5) Calculate the local mean, $\bar{m}(t) = (e_l(t) + e_u(t))/2$.
6) Subtract the local mean from $\tilde{v}(t)$, $c_i(t) = \tilde{v}(t) - \bar{m}(t)$ (i is an order of IMF).
7) Let $\tilde{v}(t) = c_i(t)$ and go to step 2); repeat until $c_i(t)$ becomes an IMF.

[1]The SVM has been often used to differentiate neural oscillations for various conditions. For example, Bathellier *et al.* showed that local cortical responses predict discrimination performance of sounds in behaving mice using SVM [16] and Wang *et al.* applied SVM to predict intended arm movement using EEG [17].

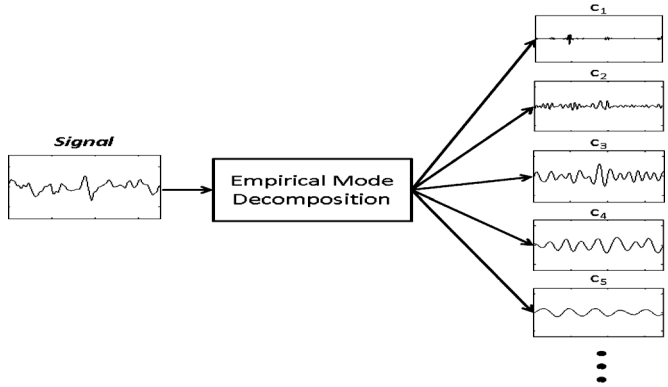

Fig. 1. An example of EMD decomposition for an input signal.

The first IMF, $c_1(t)$, is subtracted from the original signal, $v(t)$, resulting in a new signal $r(t)$. The same procedure is conducted iteratively to $r(t)$ until it contains no more oscillations. This is known as a sifting process controlled by a stopping criterion [19]. The original signal $v(t)$ is then

$$v(t) = \sum_{i=1}^{M} c_i(t) + r(t) \tag{1}$$

where $c_i(t), i = 1, \ldots, M$, are the IMFs and $r(t)$ the remaining residue. Fig. 1 illustrates an example of EMD decomposition for an input signal. The narrowband nature of the IMFs satisfies the conditions under which the Hilbert transform [7]

$$H(c_i(t)) = \frac{1}{\pi} P \int_{-\infty}^{\infty} \frac{c_i(t')}{t - t'} dt' \tag{2}$$

can be applied to obtain localized time-frequency components, where symbol P indicates the Cauchy principal value. The analytic signal is then obtained as

$$V(t) = \sum_{i=1}^{M} (c_i(t) + jH(c_i(t))) = \sum_{i=1}^{M} a_i(t) e^{j\theta_i(t)} \tag{3}$$

and is described by its amplitude and phase functions, $a_i(t)$ and $\theta_i(t)$. The phase function, $\theta_i(t)$, is differentiated to produce the instantaneous frequency, $w_i(t) = (d\theta_i(t))/(dt)$ [20].

Due to the nonlinear and nonstationary nature of EEG signals and noise, the uniqueness problem of EMD decomposition is critical to any analysis or fusion of multicomponent signals obtained in a channel-by-channel basis, since the IMFs decomposed for different EEG channels can be different in number and

frequency. This is reflected by the different decompositions produced for signals with similar statistics, and when similar frequencies appear across different IMFs, a phenomenon known as mode-mixing.

To address this problem, Rehman and Mandic [15] proposed the multivariate EMD, a natural and generic extension of the standard EMD. While standard EMD estimates the local mean using the average of upper and lower envelopes, the local mean of n-dimensional signals are computed by the multiple n-dimensional envelopes, which are generated by projecting the signal along different directions in n-variate spaces. For a uniform set of direction vectors to project the signal, low discrepancy Hammersley sequences are used to obtain quasi-uniform points on high dimensional spheres [21]. The details of MEMD[2] are outlined in Algorithm 2 [15]. The sifting process of MEMD is stopped when all the K projected signals fulfill the stoppage criterion used in standard EMD.[3]

Algorithm 2. The multivariate EMD algorithm (MEMD)

1) Choose a suitable point set for sampling on an (n-1) sphere.
2) Calculate a projection, denoted by $\{p^{\theta_k}(t)\}_{t=1}^{T}$, of the input signal $\{\mathbf{v}(t)\}_{t=1}^{T}$ along the direction vector $\mathbf{x}^{\theta_k}$, for all k (the whole set of direction vectors), giving $\{p^{\theta_k}(t)\}_{k=1}^{K}$ as the set of projections.
3) Find the time instants $t_j^{\theta_k}$ corresponding to the maxima of the set of projected signals $\{p^{\theta_k}(t)\}_{k=1}^{K}$.
4) Interpolate $[t_j^{\theta_k}, \mathbf{v}(t_j^{\theta_k})]$ to obtain multivariate envelope curves $\{\mathbf{e}^{\theta_k}(t)\}_{k=1}^{K}$.
5) For a set of K direction vectors, the mean $\mathbf{m}(t)$ of the envelope curves is calculated as $\mathbf{m}(t) = (1)/(K)\sum_{k=1}^{K}\mathbf{e}^{\theta_k}(t)$.
6) Extract the "detail" $\mathbf{c}_i(t)$ using $\mathbf{c}_i(t) = \mathbf{v}(t) - \mathbf{m}(t)$ (i is an order of IMF). If the "detail" $\mathbf{c}_i(t)$ fulfills the stoppage criterion for a multivariate IMF, apply the above procedure to $\mathbf{v}(t) - \mathbf{c}_i(t)$, otherwise apply it to $\mathbf{c}_i(t)$.

When MEMD is applied to multidimensional white Gaussian noise (WGN), the MEMD algorithm acts as a dyadic filter bank on each channel, exhibiting enhanced alignment of the corresponding IMFs from different channels across the same frequency range compared to EMD [23]. Taking advantage of this property of MEMD, a noise-assisted MEMD (NA-MEMD) was introduced by Rehman and Mandic [23] to alleviate the mode mixing problem. The NA-MEMD processes the composite signal of multivariate data and multivariate independent white noise. Therefore, the noise is never mixed with the useful data channels, since it resides in a different subspace and creates a filterbank structure to the data. This alleviates the problem of mode mixing and provides better definition of frequency bands inherent to the data. A set of IMFs corresponding to the original input data is kept by removing the IMF associated with the noise. Due to the noise channel, the scale of IMFs obeys the dyadic filter bank property, ensuring that IMFs associated with the original input data are aligned and have the same information at each level of decomposition. The details of the NA-MEMD method are described in Algorithm 3.

Algorithm 3. Noise-Assisted MEMD (NA-MEMD)

1) Create an uncorrelated white Gaussian noise time-series (q-channel) of the same length as that of the input.
2) Add the noise channels (q-channel) created in Step 1 to the input multivariate (n-channel) signal, obtaining an $(\mathrm{n}+\mathrm{q})$-channel signal.
3) Process the resulting $(\mathrm{n}+\mathrm{q})$-channel multivariate signal using the MEMD algorithm listed in Algorithm 2, to obtain multivariate IMFs.
4) From the resulting $(\mathrm{n}+\mathrm{q})$-variate IMFs, discard the q channels corresponding to the noise, giving a set of n-channel IMFs corresponding to the original signal.

B. Subjects

Ten right-handed healthy subjects (age : 20.8 ± 2.6 yrs, four men and six women) participated in the study. The study was approved by the Human Subjects Institutional Review Board of the University of California, San Diego. Written informed consent was obtained from all the subjects.

C. EEG Recordings

Scalp electroencephalographic activity was sampled continuously at 512 Hz using a 70-channel active electrode array, of which 64 channels were mounted in an elastic cap according to the extended International 10–20 system, with a DRL/CMS reference (Biosemi Inc., Amsterdam, The Netherlands). Four electrodes were mounted on the supra- and infraorbital ridges of the right eye as well as lateral to the outer canthi of the right and left eyes to measure eye movements, a technique known as electrooculography (EOG). Two electrodes were also attached to the right and left neck at the height of the seventh cervical vertebra to monitor activity of the neck muscles, particularly the trapezius. Electrode locations were digitized in 3-D space with a Fastrak system (Polhemus Inc., Colchester, VT, USA) in combination with the Locator software suite (SourceSignalImaging, San Diego, CA, USA).

D. Eye Movement Recordings

Throughout the experiment, the observer's right eye-position was recorded at 1000 Hz using the Eyelink-1000 Tower Mount (SR Research, Osgoode, ON, Canada), a noninvasive infrared video-oculographic system with a gaze resolution of $<0.01^{\circ}$ and a gaze position accuracy of $\sim 0.5^{\circ}$. The manufacturer's software was used for calibration, validation, and drift-correction. The eye–screen distance was 400 mm. Events and TTL time

[2]The MATLAB code of MEMD is available from http://www.commsp.ee.ic.ac.uk/~mandic/research/emd.htm.

[3]We employed a combination of EMD stoppage criteria, given in [19] and [22], for MEMD sifting.

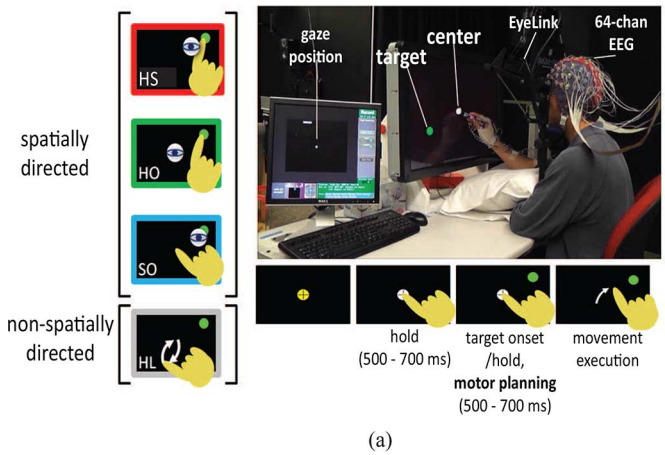

Fig. 2. Experiment setup and targets on the screen. While subjects conducted spatially directed movements (both hand and eyes "HS," only their hand "HO" or only their eyes "SO") and nonspatially directed movement (hand lift "HL") following a 500–700 ms hold interval, the positions of hand and eyes, and EEG were synchronously recorded. (a) Experiment setup. (b) Targets on the screen.

pulses sent from the stimulation computer were recorded and saved in conjunction with the eye position data.

E. Hand and Arm Motion Capture

Three-dimensional movement kinematics of the right hand and arm were recorded at 120 Hz or 240 Hz via 10 infrared LED sensors (PhaseSpace, Inc., San Leandro, CA, USA) securely attached to the stylus (three sensors) and back of the hand (4 sensors), as well as wrist, elbow, and shoulder (one sensor each) of the participant. The middle stylus sensor was used for reconstructing finger position as well as hand onset and offset latencies. Data was recorded continuously together with a TTL master time stamp sent from the stimulation computer (see [24] for more details).

F. Experimental Paradigm

Subjects sat in front of a 32 in touch screen at an angle of 85° with respect to the horizontal axis (AccuTouch, Elo TouchSystems, Menlo Park, CA, USA) and were requested to perform time-constrained reaching and/or eye movements from the center of the touch-screen to a lateral target (see Fig. 2). Viewing distance was held constant at 400 mm with a chin rest. We used a simplified task introduced by [25]–[27]. Over the course of the experiment, we varied the movement modality and the amount of eye–hand coordination: Subjects either had to touch the target while being allowed to freely move their eyes (condition "hand+saccade," HS), touch the target while maintaining fixation at the center (condition "hand only," HO), saccade towards

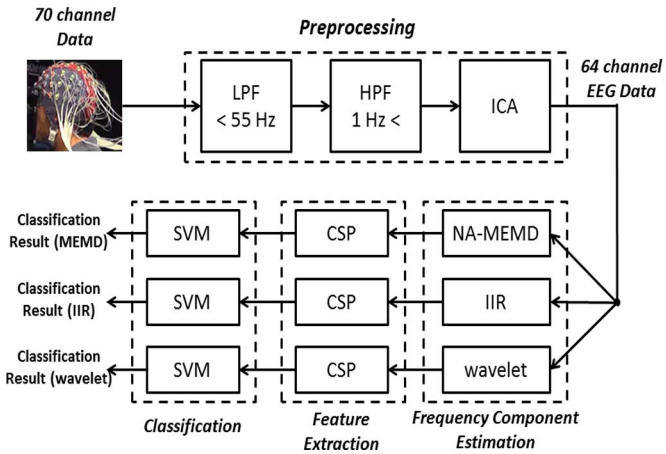

Fig. 3. Signal processing block diagram to produce the classification results using the noise-assisted MEMD, IIR filter, and wavelet (Morlet). LPF and HPF denote low-pass filter and high-pass filter, respectively.

the target while holding their hand at the center (condition "saccade only," SO), or to simply lift their hand from the screen and bring it back to the former center location (condition "hand lift," HL). In all conditions, lateral target discs were presented. As depicted in Fig. 2, subjects initiated a trial by touching and looking at the center fixation cross, which resulted in a center color change from yellow to white. After a randomized time interval ranging between 500 and 700 ms, a lateral target, colored green, was presented in either the lower left or upper right area of the screen. Subjects were required to maintain their fixation and hand at the center. This "hold" interval was active for a randomized time interval of 500–700 ms. Whenever subjects moved their hand and/or eyes prematurely, the center turned again yellow and the trial was re-initiated with a newly randomized target. Upon successful completion of the hold interval, the center disc disappeared, signaling the subject to perform the requested movement within a time window which was determined in a training session of 100 "hand+saccade" trials preceding the main experiment (four subjects: 450 ms; six subjects: 500 ms). Hand or eye endpoints, i.e., the point where the stylus/gaze hit the touch screen, were displayed as small white dot (radius of 10 pixels $=$ 5 mm) together with an auditory cue for 200 ms (differentiating between target hits, misses, and time-outs). Hits, misses, and time-outs (responses exceeding the time constraint) yielded monetary gains or losses. We analyzed the 500 ms interval of "motor planning" following the "go" signal before the movement execution took place in order to examine changes in the neural dynamics during the four different conditions of movement planning. There were about 100 trials to left and right targets for "HS," "HO," and "SO" conditions and 50 trials for the "HL" condition.

G. Signal Processing for Classification

Fig. 3 illustrates the block diagram from preprocessing the 70 channel data to the calculation of classification results using the three different frequency component estimation methods [noise-assisted MEMD, infinite impulse response (IIR) filter, and wavelet transform (Morlet)].

1) Preprocessing: In order to remove motion artifact and ambient noise, a preprocessing procedure was performed on the continuous data using EEGLAB software [28]. The continuous

EEG signal was low-pass filtered below 55 Hz and high-pass filtered over 1 Hz using an IIR filter, removing the power line noise (60 Hz) and dc offset. Afterwards the continuous EEG signal was epoched into segments of 1.4 s based on target onset latencies (from -200 to 1200 ms after the target onset). Bad epochs were visually rejected by observing burst movements or large contractions of head and neck muscles. After that, independent component analysis (ICA) [29] was applied to remove the stereotyped artifacts such as blinks, eye movements, and motion [30]. For those artifact rejection, we used InfoMax ICA [31], [32], which aims to minimize mutual information between sources by maximizing entropy. Independent Components (ICs) were analyzed with respect to scalp topography and frequency characteristics, and those that displayed features indicative of artifacts were removed. For example, muscle artifacts were identified by ICs having a spatially focal scalp projection and high power at high frequencies (20–50 Hz and above). The ICs were derived from the full set of trials (i.e., $\mathrm{HS}+\mathrm{HO}+\mathrm{SO}+\mathrm{HL}$), which is a standard procedure [33].

2) Frequency Component Estimation: The 64 channel EEG data of the preprocessed 70 channel data was decomposed simultaneously using NA-MEMD with the aid of three additional noise channels, where the ratio between the standard deviation of the noise and data was 0.1 [8]. Based on the average power spectra of each IMF across channels and subjects, IMFs related to gamma, beta, alpha, and theta rhythms were defined. A comparative study was performed to show the ability of NA-MEMD to produce more accurate frequency component estimates over the IIR filter and wavelet transform. A sixth-order Butterworth IIR filter was designed for the high-pass filter (30 Hz <), which is commonly used for EEG analysis [34], [35]. The wavelet transform[4] (widely used Morlet wavelet [7]) were applied and the scales were reconstructed to obtain the high-pass filtered signals.

3) Common Spatial Patterns: Features relevant to motor planning were extracted using the common spatial patterns (CSP) algorithm, often used in BCI applications [36], [37]. It provides spatial filters that maximize the variance of signals in one class and simultaneously minimize the variance of signals in the other class. In this way, CSP filters can classify between ERD/ERS caused by changing brain dynamics, since their operation is sensitive to subtle changes in the power of band-pass filtered data. For a detailed description of the CSP algorithm, see Appendix A.

4) Classification: The feature vectors $\mathbf{f} = [f_1, f_2, f_{63}, f_{64}]$, obtained by (11) in Appendix A for $m = 2$ (m defines the number of spatial filters)[5], were classified using a support vector machine (SVM) [18] with a Gaussian kernel.[6] The trial data for each task was divided into 80% training and 20% testing sets,[7] and the classification was repeated five times while changing the sample order. The average of these outcomes was the final classification rate (five-fold cross-validation). The 95% upper limit of confidence interval between two classes was obtained through bootstrapping with 2500 replications of random label reshuffling.

[4]The wavelet transform is given by

$$\bar{W}(\dot{a}, \dot{b}; V, \psi) = |\dot{a}|^{-1/2} \int_{-\infty}^{\infty} V(t)\psi^* \left(\frac{t-\dot{b}}{\dot{a}}\right) dt \tag{4}$$

where ψ^* is the mother wavelet, $\dot{a}$ the dilation factor, and $\dot{b}$ the translation of the origin.

[5]Two most important spatial filters were the optimal number of filters and the use of more filters did not significantly improve classification accuracy [36].

[6]If complete model selection using the Gaussian kernel has been conducted, there is no need to consider linear SVM [38]. The MATLAB code can be downloaded from [39].

H. Event-Related (De)Synchronization

In order to look into the power feature of frequency components, we used event-related (de)synchronization (ERD/ERS) [40], which is the relative changes in power relative to the baseline power and is defined as

$$\mathrm{ERD/ERS} = \frac{A-R}{R} \times 100\% \tag{5}$$

where A is the power within the frequency band of interest in the period after the event, and R is that of the preceding baseline period. ERD/ERS was investigated within four frequency bands: theta (4–8 Hz), alpha (8–13 Hz), beta (13–30 Hz), and gamma (30–55 Hz). IMFs within these frequency bands were chosen by the average power spectra of the IMFs across all data. The power of IMFs were estimated using the squared value of instantaneous amplitude in (3), $(a_i^2(t))/(2)$.

III. Results

A. IMFs of EEG

Fig. 4 illustrates the first seven IMFs decomposed using NA-MEMD corresponding to channels F3, F4, C3, C4, P3, and P4. Note that the common oscillatory modes are aligned at the same IMF level without mode mixing across IMFs. c_1 has the highest frequency components while c_7 has the lowest components. Spectral estimation of each IMF was calculated using a periodogram (Bartlett window) [41]. Average power spectra across all channels for all trials and all subjects are illustrated in Fig. 5. Notice that gamma band rhythm can be estimated from c_1 and c_2, beta band rhythm from c_3, alpha band rhythm from c_4, and theta band rhythm from c_5. Fig. 5(b) is an enlarged image of power spectrum for the sum of c_1 and c_2. For the comparison with wavelet and IIR filter, the average power spectra of the gamma band signals produced using wavelet and IIR filter are also illustrated in the same figure.

B. Event-Related Synchronization Using IMFs

Grand average of event-related synchronization (ERS) topoplots [42] for all 10 subjects were calculated using the IMFs corresponding to different motor tasks (Fig. 13). The ERS topoplot shows power changes during the motor planning period (0 to $\sim$ 500 ms) relative to the average of the baseline period (-200 to $\sim$ 0 ms). Warmer colors indicate an increase in power on the channel after the stimulus onset. The gamma rhythm IMFs, c_{1-2} (sum of c_1 and c_2), have more spatial dynamic variation across tasks to both left and right targets as compared to the other IMFs. For example, ERS of "HS" has strong activity on temporal and posterior areas, while the ERS of "HL" and 'HO' show power increase on the frontal channels.

[7]The CSP filter parameters were defined using only the training data set.

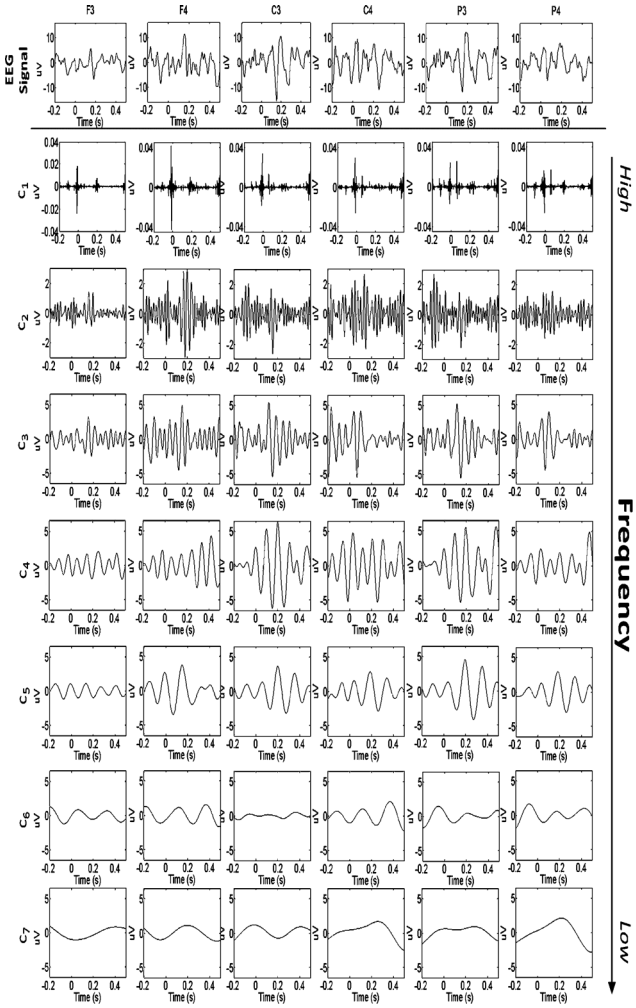

Fig. 4. Decomposition of EEG signals from six channels using the noise-assisted MEMD. Note that each IMF contains a single frequency mode. IMF contains slower oscillation as the index of IMF is increased.

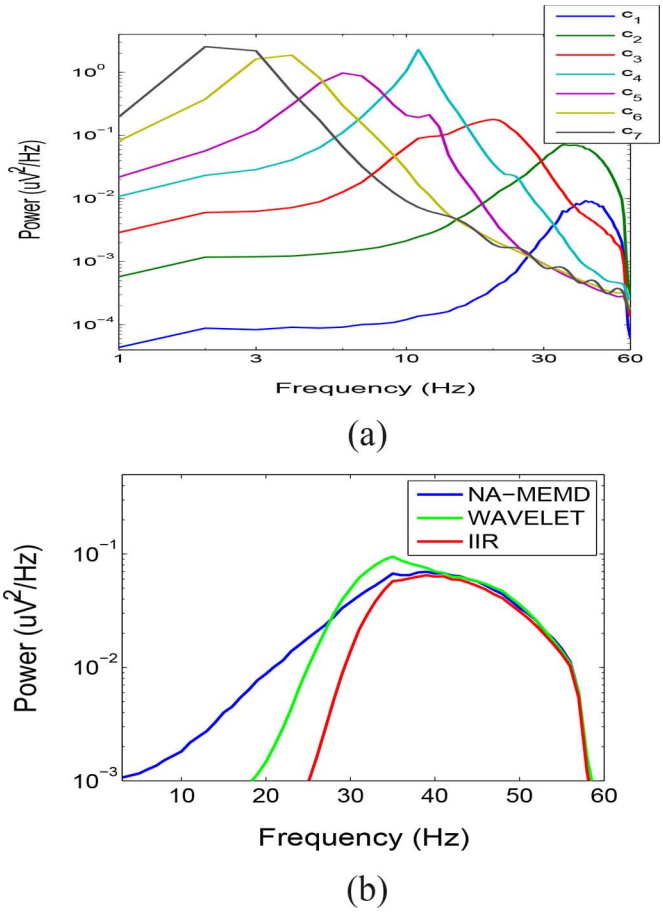

Fig. 5. Average power spectra of c_1–c_7 across channels and subjects. Each IMF works as a filter bank, where c_1 and c_2 contain most of gamma band, c_3 beta band, c_4 alpha band, c_5 theta band, and c_6 and c_7 delta band components. Note the comparison of the gamma band power spectra using different algorithms in (b). (a) Power spectra of c_1–c_7. (b) Power spectra of gamma band.

Other IMFs, including c_{1-7} (sum of IMFs from c_1 to c_7, which contains frequency components from 1 to 55 Hz based on Fig. 5), reflect significant changes in the posterior and occipital regions. We studied the significance of the difference of spatial power distribution across the four different motor preparation conditions. The 64 channel ERS values were normalized, and the difference of the values between pairs of tasks was tested using a t-test. Fig. 14 illustrates the p-values for each channel, for all pairwise combinations of motor tasks. The number of significant channels (p-values less than 0.05) is reported under each topoplot. Overall, the gamma rhythm ERS using c_{1-2} had more significantly different channels than the other IMFs shown. This finding suggests that the spatial information in multichannel EEG used for classification of the different motor conditions derives mostly from the gamma rhythm IMFs.

C. Single Trial Classification Results

Instead of trial averaging (as in the ERS analysis), the IMFs corresponding to the four motor tasks were classified using CSP with SVM in order to investigate the spatial information of the multichannel EEG in single trials. Tables I and II show the classification results of all combinations of four motor planning tasks to left and right targets using c_{1-2}. The classification rates above 95% confidence interval determined by a bootstrapping method are indicated in bold. As an index of behavioral performance for each subject, average 2-D Err (Error) to the target was recorded while subjects executed hand movement with saccade. Overall, the subjects who had good performance with smaller "2D Err" had higher classification rates, such as subjects 4, 5,

TABLE I
CLASSIFICATION RESULTS (IN %) PRODUCED USING c_{1-2}, MOSTLY GAMMA BAND COMPONENTS, BETWEEN TWO DIFFERENT CONDITIONS FOR "LOWER LEFT" TARGET. "HS" DENOTES HAND WITH SACCADE, "HL" HAND LIFT, "HO" HAND ONLY, "SO" SACCADE ONLY AND "2D ERR" 2-D ERROR DURING HAND MOVEMENT WITH SACCADE. CLASSIFICATION RATES ABOVE 95% CONFIDENCE INTERVAL DETERMINED BY A BOOTSTRAPPING METHOD ARE INDICATED IN BOLD. NOTE THE SUBJECTS HAVING WORSE CLASSIFICATION RATES PRODUCED HIGHER 2-D ERRORS, SUCH AS SUBJECT 1, 3, AND 9

Subject	HS vs HL	HS vs HO	HS vs SO	HO vs SO	HO vs HL	SO vs HL	MEAN	2D Err
1	**60.67**	**53.53**	**51.67**	46.67	**53.33**	51.54	52.90	0.75
2	**66.21**	**64.10**	**92.00**	**58.82**	**74.29**	**70.00**	70.90	0.69
3	**67.14**	**55.68**	**72.41**	**70.77**	**69.60**	47.06	63.78	0.93
4	**72.67**	**66.32**	**71.33**	**82.10**	**75.71**	**71.00**	73.195	0.48
5	**65.33**	**64.50**	**83.33**	**76.70**	**76.00**	**87.69**	75.59	0.64
6	**73.57**	**66.86**	**65.46**	**60.00**	**63.48**	**55.24**	64.10	0.69
7	**68.67**	**86.67**	**78.42**	**71.20**	**76.15**	**83.57**	77.44	0.42
8	**68.28**	**79.43**	**67.50**	47.40	53.33	**66.21**	63.70	0.68
9	**72.14**	**57.14**	**60.57**	**53.30**	**62.61**	56.52	60.39	0.76
10	**80.00**	**70.50**	**81.67**	**58.33**	**66.67**	**62.31**	69.91	0.78
MEAN	69.47	66.47	72.44	62.50	67.12	65.11		

TABLE II
CLASSIFICATION RESULTS (IN %) PRODUCED USING c_{1-2}, MOSTLY GAMMA BAND COMPONENTS, BETWEEN TWO DIFFERENT CONDITIONS FOR "UPPER RIGHT" TARGET. "HS" DENOTES HAND WITH SACCADE, "HL" HAND LIFT, "HO" HAND ONLY AND "SO" SACCADE ONLY. "HS" DENOTES HAND WITH SACCADE, "HL" HAND LIFT, "HO" HAND ONLY, "SO" SACCADE ONLY AND "2D ERR" 2-D ERROR DURING HAND MOVEMENT WITH SACCADE. CLASSIFICATION RATES ABOVE 95% CONFIDENCE INTERVAL DETERMINED BY A BOOTSTRAPPING METHOD ARE INDICATED IN BOLD. NOTE THE SUBJECTS HAVING WORSE CLASSIFICATION RATES PRODUCED HIGHER 2-D ERRORS, SUCH AS SUBJECT 3, 8, AND 9

Subject	HS vs HL	HS vs HO	HS vs SO	HO vs SO	HO vs HL	SO vs HL	**MEAN**	**2D Err**
1	**72.86**	**57.00**	**55.00**	**51.00**	**71.43**	**72.86**	63.36	0.65
2	**77.86**	**85.13**	**93.89**	**55.40**	**78.52**	**75.83**	77.78	0.62
3	**71.33**	**55.50**	**57.37**	**74.20**	**61.33**	**70.71**	65.08	0.81
4	**78.57**	**60.54**	**79.39**	**73.30**	**79.20**	**81.91**	75.49	0.46
5	**71.11**	**63.03**	**82.16**	**80.70**	**76.00**	**85.83**	76.47	0.69
6	**72.59**	**64.62**	**67.14**	**71.00**	61.43	**68.24**	67.51	0.69
7	**70.00**	**80.00**	**79.44**	**71.50**	**76.80**	**77.50**	75.88	0.60
8	**74.62**	**62.94**	56.00	**55.80**	**66.00**	52.50	61.32	0.75
9	**73.33**	**53.51**	**65.88**	**51.00**	**55.56**	**60.00**	59.88	0.84
10	**81.43**	**78.34**	**80.56**	45.5	**68.00**	49.17	67.16	0.68
MEAN	74.37	66.06	71.68	62.90	69.43	69.46		

and 7 to the left target in Table I and subjects 2, 4, and 7 to the right target in Table II. The correlation analysis between classification rates and "2D Err" will be addressed below.

The classification results using the other IMFs were calculated and their averages across subjects are shown in Fig. 6 with standard errors (error bars). Overall, the average classification rates using c_{1-2} were the highest. The classification results using a sum of all the IMFs, c_{1-7} (1–55 Hz), were largely outperformed by c_{1-2}. For rigor, the higher classification rate using c_{1-2} compared to the other IMFs was analyzed using the one-tailed t-test, and the significant cases are denoted using stars on the error bars of c_{1-2} classification results. The different colors of the stars illustrate the significant improvement of c_{1-2}, p-values less than 0.05, compared to the different IMFs (i.e., green star to c_3, red to c_4, cyan to c_5, and black to c_{1-7}). Overall, c_{1-2} produced higher classification rates than the others for the six different scenarios, which infers that gamma rhythm c_{1-2} contains significantly larger amount of information to classify the four motor tasks than the other frequency band IMFs. We also used the receiver-operating characteristic (ROC) analysis [43] to assess the classification performance of the IMFs, plotting the sensitivity (true positive rate) of classification against the false-positive rate. For example, when we discriminate between "HS" and "HL," the sensitivity refers to the percentage of trials which was classified as "HS" among all "HS," and the false-positive rate refers to the percentage of trials which was classified as 'HS' among all "HL." The area under the ROC curve (AUROC) is a measure of how well the IMFs of two motor tasks can be separated. If the sensitivity increases steeply as the threshold for classifier increases, with a relatively small increase of false-positive results, the AUROC will become large. On the contrary, if the sensitivity grows slowly as the classifier threshold increases, with a steep increase of false-positive results, the AUROC will be small. The difference of five AUROCs of c_{1-2}, c_3, c_4, c_5, and c_{1-7} were tested to demonstrate that advantage of separation by c_{1-2} is statistically significant. Fig. 7 shows the ROC curves for the classification performance of subject 7 using c_{1-2}, c_3, c_4, c_5, and c_{1-7}. Note that the AUROCs of c_{1-2} are larger than the other AUROCs.

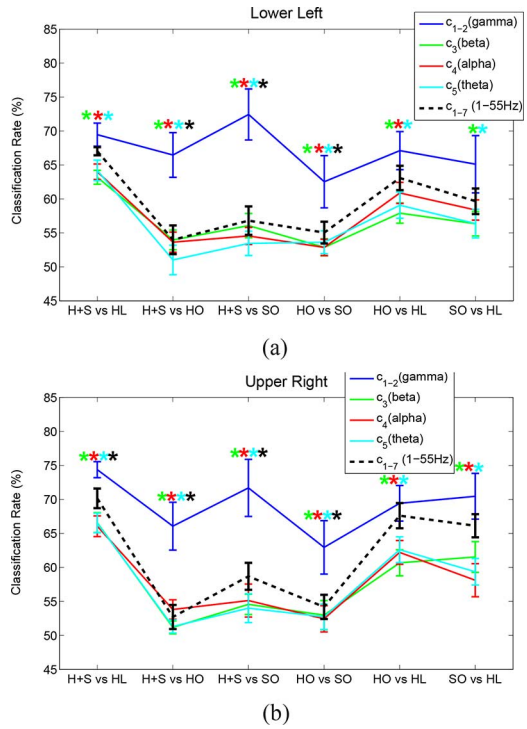

Fig. 6. Classification results between two different conditions using IMFs. Error bars illustrate the standard errors. Overall, classification rates using the sum of c_1 and c_2, gamma band components, are higher than those produced using the other IMFs including the sum of all IMFs, c_{1-7} (1–55 Hz). This is confirmed by the one-tailed t-test and the stars in different colors on the error bars display the significant improvement of c_{1-2}, p-values less than 0.05 (green star for "c_{1-2} versus c_3," red for "c_{1-2} versus c_4," cyan for "c_{1-2} versus c_5," and black for "c_{1-2} versus c_{1-7}"). (a) Lower left target. (b) Upper right target.

The AUROCs for all subjects were compared, and their averages across all subjects are shown in Fig. 8 with standard errors (error bars). Except "HO versus HL" for "Upper Right" target, the AUROCs of c_{1-2} are always significantly larger than the others for all scenarios based on the stars in the figure, which confirm the significant improvement of c_{1-2} using one-tailed t-test (p-values less than 0.05).

To compare the performance of NA-MEMD with other frequency decomposition algorithms, we classified the gamma band rhythms in the four motor tasks, using IIR and wavelet (Morlet). All 60 classification rates for 10 subjects and six combinations of motor tasks were computed, and their averages across all subjects are illustrated in Fig. 9 with standard errors and statistical significance of the performance of NA-MEMD compared to IIR and wavelet. In most of scenarios, NA-MEMD outperformed the other methods with higher mean of classification rates. In particular, the stars in the figures confirmed that NA-MEMD extract significantly more information to separate the different motor tasks than wavelet for many cases. On the other hand, the higher performance of NA-MEMD compared to IIR was not significant and the mean classification rates of IIR were higher than wavelet. The preprocessed EEG signals using highpass (1 Hz<) and lowpass (<55 Hz) filter were linear due to the filters designed based on Fourier theory [10] and thus IIR filter, by design, was suitable for linear signal statistics. In addition, the problem with the wavelet is its leakage generated

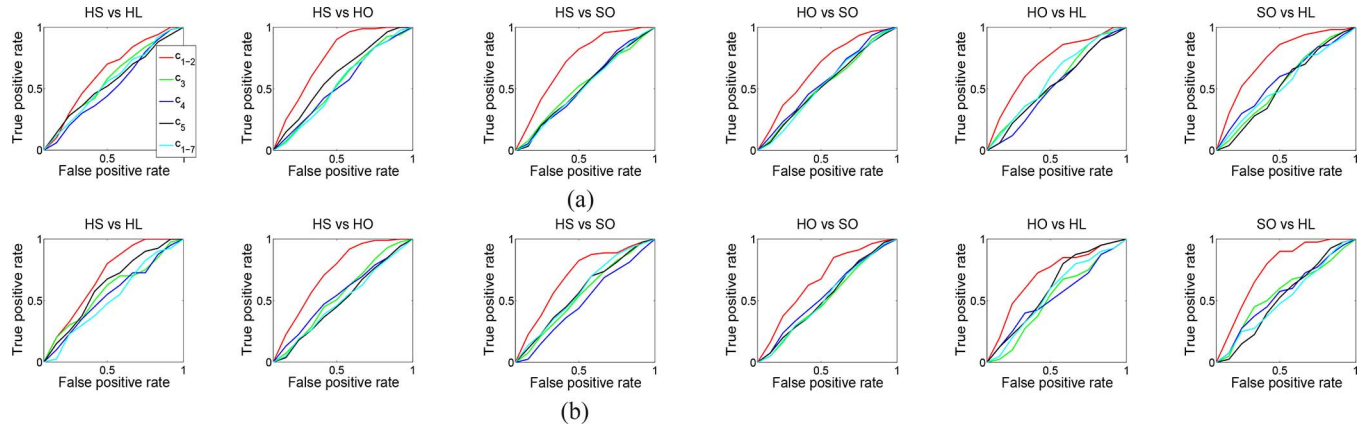

Fig. 7. ROC curves for the classification performance of subject 7, produced using c_{1-2}, c_3, c_4, c_5, and c_{1-7}. Overall, ROC curves of c_{1-2} attain smaller false-positive and false-negative probabilities across the whole sweep of classification boundaries than the others. (a) Lower left target. (b) Upper right target.

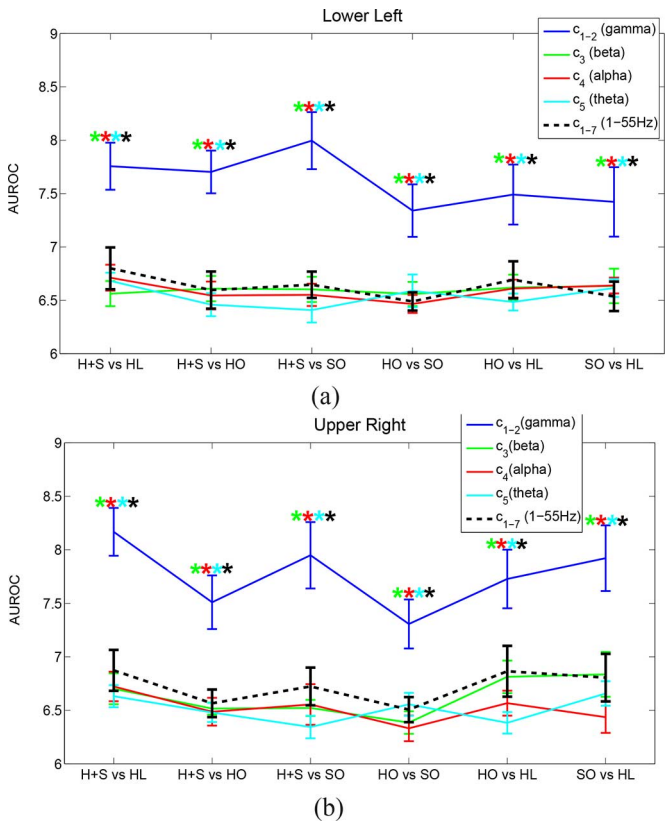

Fig. 8. AUROC results between two different conditions using IMFs. The error bars illustrate the standard errors. Overall, AUROCs using the sum of c_1 and c_2, gamma band components, are higher than those produced using the other IMFs including the sum of all IMFs, c_{1-7} (1–55 Hz). This is confirmed by the one-tailed t-test and the stars in different colors on the error bars display the significant improvement of c_{1-2}, p-values less than 0.05 (green star for "c_{1-2} versus c_3" red for "c_{1-2} versus c_4," cyan for "c_{1-2} versus c_5," and black for "c_{1-2} versus c_{1-7}"). (a) Lower left target. (b) Upper right target.

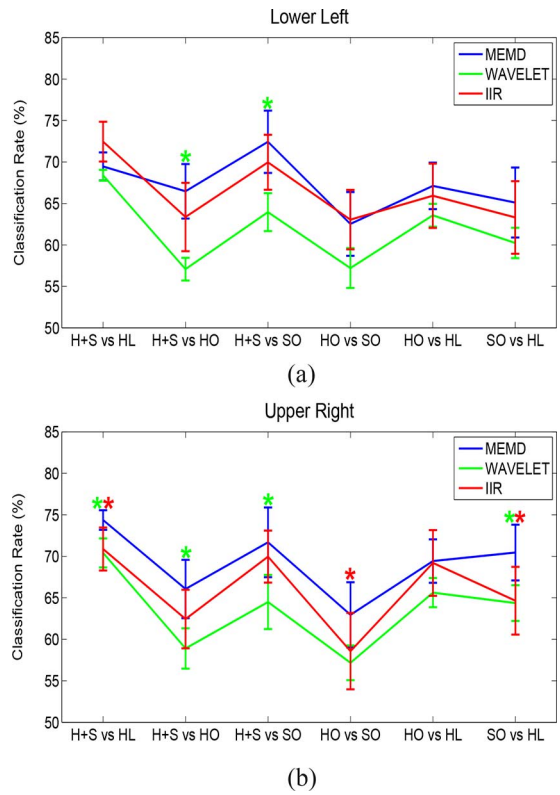

Fig. 9. Classification results between two different conditions using NA-MEMD, IIR, and wavelet (Morlet). The error bars illustrate the standard errors. Overall, the averages of the classification rates using NA-MEMD are higher than those produced using the other methods. In many cases, NA-MEMD outperformed the wavelet decomposition significantly, denoted by the stars in green color. (a) Lower left target. (b) Upper right target.

by the limited length of the basic wavelet function [7], and Sørensen *et al.* demonstrated IIR outperformed wavelet depending on the amount of noise [44]. The ROC curves for the classification performances of NA-MEMD, IIR and wavelet were also calculated and Fig. 10 shows the ROC curves for the classification performance of subject 7. Overall, the AUROCs of NA-MEMD look larger than the others. The AUROCs for all 10 subjects calculated using the three algorithms were compared and the averages across all subjects are shown in Fig. 11. Similar to classification results, the highest means of AUROCs were obtained using NA-MEMD, and wavelet was significantly outperformed by NA-MEMD for all six scenarios.

D. Prediction of Behavior Using Gamma Rhythm

We also investigated the prediction of behavior using classification results of the gamma rhythm (c_{1-2}) by calculating

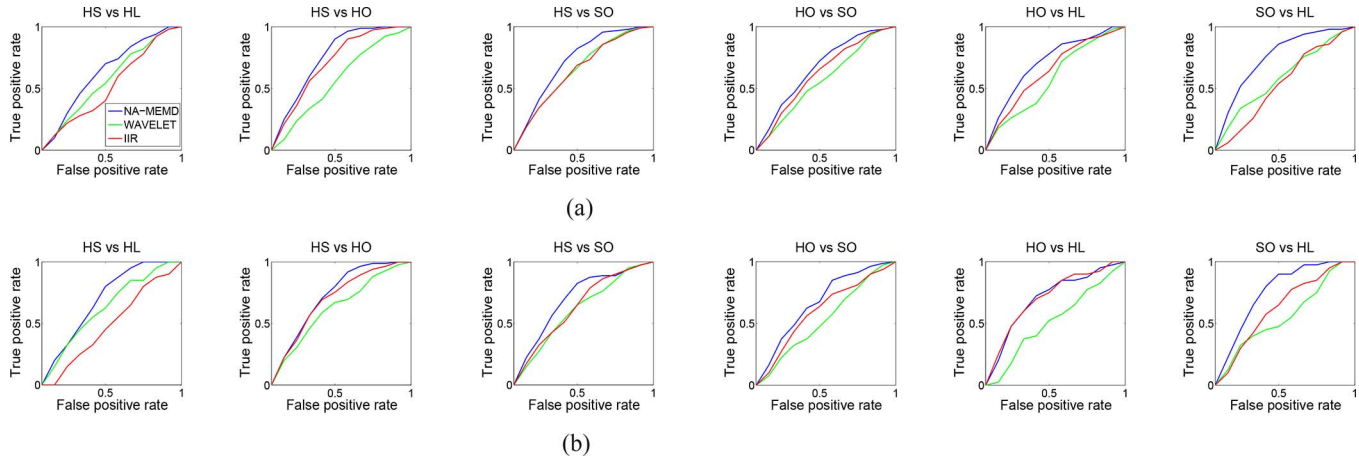

Fig. 10. ROC curves for the classification performance of subject 7, produced using NA-MEMD, IIR filter, and wavelet (Morlet). Overall, ROC curves of NA-MEMD attain smaller false-positive and false-negative probabilities across the whole sweep of classification boundaries than the others. (a) Lower left target. (b) Upper right target.

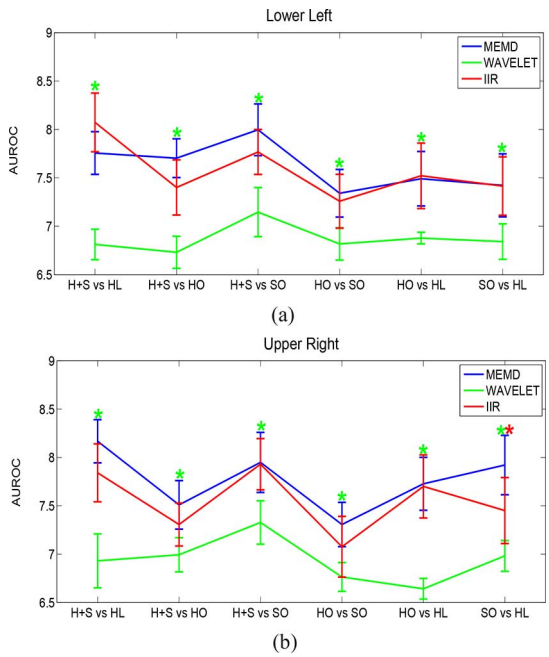

Fig. 11. Results of AUROCs between two different conditions using NA-MEMD, IIR and wavelet (Morlet). Error bars illustrate the standard errors. Overall, the averages of the AUROCs using NA-MEMD are higher than those produced using the other methods. In most cases, NA-MEMD outperformed the wavelet decomposition significantly, denoted by the stars in green color. (a) Lower left target. (b) Upper right target.

the correlation between classification rates and average behavioral performance (2-D error of "HS"). Classification results included only "HS" tasks (i.e., "HS versus HL," "HS versus HO," and "HS versus SO" in Tables I and II were only considered). Fig. 12(a) plots the correlation between the average hand to target 2-D error (distance) for all "HS" trials and the average classification rates of "HS versus HL," "HS versus HO," and "HS versus SO." The red and blue dots correspond to the lower left and upper right targets, respectively, for all subjects. The cases of lower left target and upper right target had meaningful correlation coefficients of -0.47 and -0.52, and the correlation coefficient for both targets was significant, -0.48 ($p < 0.05$).

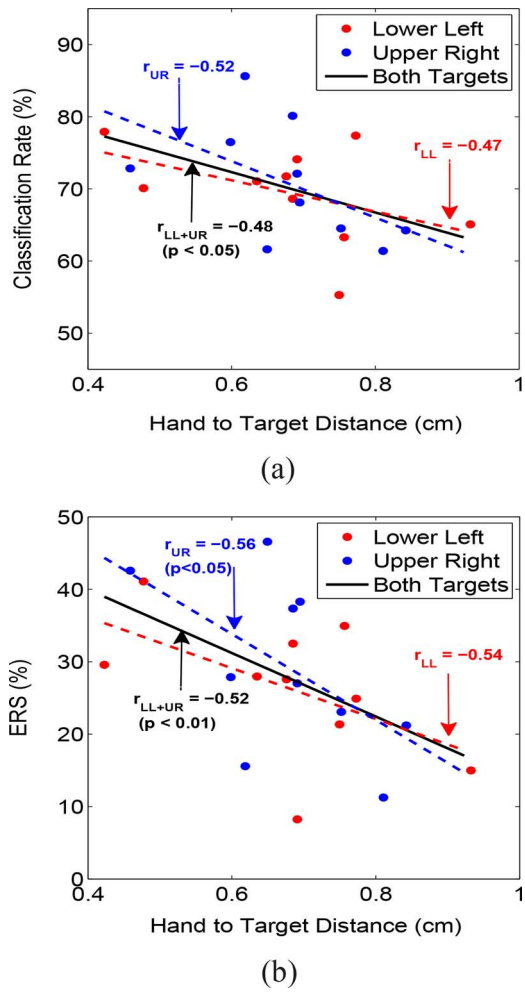

Fig. 12. Correlations (a) between gamma band classification rates and behavior (2-D error), and (b) between gamma band ERS produced using NA-MEMD and behavior. Note that the correlation coefficients are significant for both targets, which means gamma rhythm during movement preparation can predict movement. (a) Classification versus Behavior (2-D Err). (b) ERS versus Behavior (2-D Err).

The correlation coefficients between behavioral performance and classification rates using different frequency rhythms are

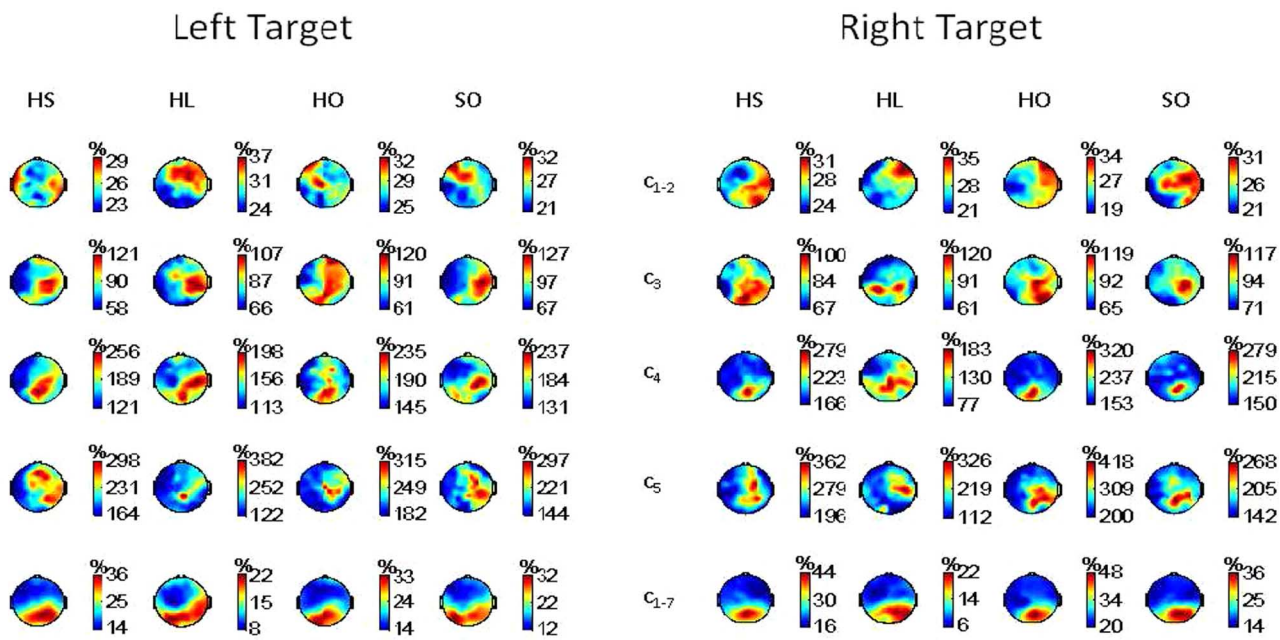

Fig. 13. Event-related synchronization between 0 ms and 500 ms (movement planning) estimated using IMFs of NA-MEMD. "HS" denotes hand with saccade, "HL" hand lift, "HO" hand only and "SO" saccade only. Note the more dynamic spatial differences in gamma band (c_{1-2}) corresponding to the different conditions compared to the other bands including c_{1-7}.

TABLE III
CORRELATION BETWEEN CLASSIFICATION RATES PRODUCED USING NA-MEMD AND BEHAVIOR (2-D ERROR DURING "HS" TASK). SIGNIFICANT CORRELATION RATES ($p < 0.05$) ARE INDICATED IN BOLD. NOTE THE CLASSIFICATION RATES OF c_{1-2}, MOSTLY GAMMA BAND COMPONENTS, ARE SIGNIFICANTLY CORRELATED WITH BOTH BEHAVIORAL PERFORMANCES TO THE LEFT AND RIGHT STIMULI

	R_{LEFT}	R_{RIGHT}	$R_{LEFT+RIGHT}$
c_{1-2}	-0.47	-0.52	**-0.48**
c_3	0.30	-0.33	0.08
c_4	0.10	-0.19	-0.04
c_5	0.18	-0.00	0.10
c_{1-7}	0.27	-0.12	0.08

TABLE IV
CORRELATION BETWEEN GAMMA BAND CLASSIFICATION RATES, PRODUCED USING NA-MEMD, IIR, AND WAVELET (MORLET), AND BEHAVIOR (2-D ERROR DURING "HS" TASK). THE SIGNIFICANT CORRELATION RATES ($p < 0.05$) ARE INDICATED IN BOLD. NOTE THE CLASSIFICATION RATES PRODUCED USING NA-MEMD ARE HIGHER THAN THE OTHERS

	R_{LEFT}	R_{RIGHT}	$R_{LEFT+RIGHT}$
NA-MEMD	-0.47	-0.52	**-0.48**
IIR	-0.47	-0.35	**-0.41**
wavelet	-0.02	-0.51	-0.24

reported in Table III. Unlike the significant correlation coefficients for gamma rhythm c_{1-2}, the correlation coefficients for the other IMFs had low correlation coefficients. These results imply that the gamma rhythm during motor planning had most significant information about the four different motor tasks for predicting hand movements. Table IV answers the question of which algorithm (NA-MEMD, IIR, and wavelet) could extract the most accurate gamma rhythm for predicting the behavior of the subjects using the correlation coefficients for gamma rhythm classification across all algorithms and performance characteristics. Among the three algorithms, NA-MEMD had the highest correlation for $R_{LEFT+RIGHT}$ (p-values less than 0.05).

TABLE V
CORRELATION BETWEEN EVENT-RELATED SYNCHRONIZATION (ERS) ON P6 PRODUCED USING NA-MEMD AND BEHAVIOR (2-D ERROR DURING "HS" TASK). SIGNIFICANT CORRELATION RATES ($p < 0.05$) ARE INDICATED IN BOLD. NOTE THE ERS OF c_{1-2}, MOSTLY GAMMA BAND COMPONENTS, HAS HIGHER CORRELATION COEFFICIENTS THAN THE OTHERS

	R_{LEFT}	R_{RIGHT}	$R_{LEFT+RIGHT}$
c_{1-2}	-0.54	**-0.56**	**-0.52**
c_3	-0.40	0.07	-0.23
c_4	0.01	-0.37	-0.17
c_5	0.21	-0.16	0.05
c_{1-7}	-0.39	**-0.57**	**-0.46**

In our previous study [45], increased amplitude in the vicinity of 300 ms after stimulus onset (P300) was found in the parietal area for planning spatially directed movement separation. Werf *et al.* [4], [5] showed gamma band power enhancement over the parietal region during spatial attention of saccade and movement planning using magnetoencephalography (MEG). We looked into the gamma band power enhancement, ERS, during "HS" task (Fig. 13). We found that ERS in parietal region, particularly P6, was correlated with behavioral performance of subjects, hand to target 2-D error.[8] Similar to the correlation coefficient between gamma band classification rates and behavioral performance in Fig. 12(a) and (b) contains the scatter plot of ERS on P6 versus hand to target distance errors, for every subject and target. The correlation coefficient for the left target is -0.54, for the right target it is -0.56, and for both targets it is -0.52, each of which is significant ($p < 0.05$). This result indicates that more spatial attention to the targets increases gamma band power in the parietal area. Table V shows the correlation coefficients between ERS calculated

[8]This correlation method was used by Lenz *et al.* to show the relationship between gamma band response in parieto-occipital region and performances of healthy children and patients with attention-deficit/hyperactivity disorder [46].

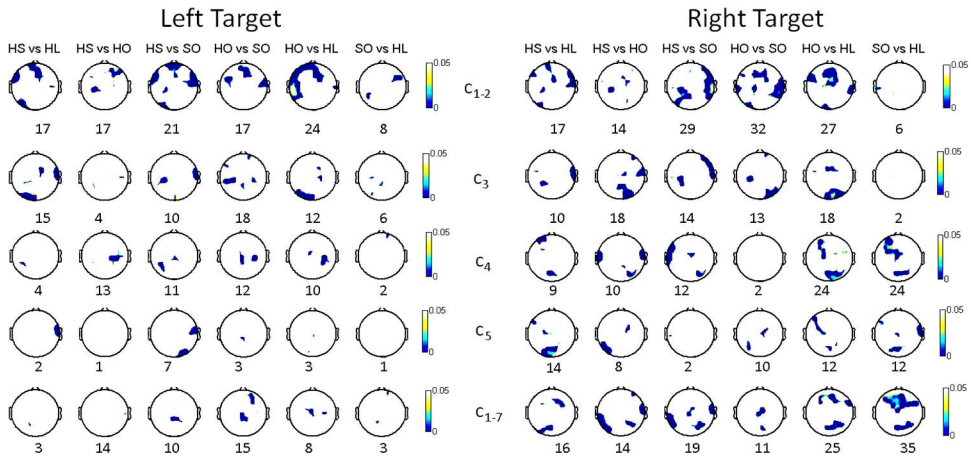

Fig. 14. p-value topoplots using a t-test for the difference of IMF powers between two conditions. Numbers under topoplots denote the number of channels whose p values are less than 0.05. In general, the topoplots of c_{1-2} have more number of significantly different channels than the others.

TABLE VI
CORRELATION BETWEEN GAMMA BAND ERS RATES, PRODUCED USING NA-MEMD, IIR, AND WAVELET (MORLET), AND BEHAVIOR (2-D ERROR DURING "HS" TASK). SIGNIFICANT CORRELATION RATES ($p < 0.05$) ARE INDICATED IN BOLD. NOTE THE CLASSIFICATION RATES PRODUCED USING NA-MEMD ARE HIGHER THAN THE OTHERS

	R_{LEFT}	R_{RIGHT}	$R_{LEFT+RIGHT}$
NA-MEMD	-0.54	**-0.56**	**-0.52**
IIR	-0.29	-0.14	-0.21
wavelet	0.08	0.11	0.08

using the other IMFs and behavioral performances of subjects. Overall, the results of gamma band ERS using c_{1-2} are higher than the others. The correlation coefficients calculated using IIR and wavelet were also estimated in Table VI, and they demonstrated only NA-MEMD could produce the significant ERS predicting the behavior of the subjects.

IV. DISCUSSION

We presented the changes of neural oscillations during the planning of spatially (or nonspatially) directed reaches and saccades using MEMD with a classification tool, SVM. Analysis of EEG during the motor planning interval revealed that the gamma band provided more information about the upcoming movement than the other frequency bands. In addition, MEMD provided higher levels of accuracy in classifying the different tasks, based on the EEG, than did traditional signal processing methods such as Fourier and wavelet transforms. Moreover, the reaching accuracy of subjects after these motor planning periods was significantly correlated with the separation rates, which confirmed the accurate extraction of gamma band rhythm corresponding to the tasks using MEMD. Furthermore, the correlation between the power feature of gamma rhythm over the parietal cortex and reaching accuracy also demonstrates the significance of the gamma rhythm in planning spatially directed movements.

What role might gamma oscillations play in spatially directed movements? Although most studies of gamma oscillations have focused on nonmotor functions, demonstrating the involvement of gamma oscillations in attention and memory [47], [48], there is a small but growing literature on the role of gamma oscillations in motor control. Brown *et al.* have suggested that gamma oscillations are prokinetic, facilitating the production of movement in general [49], [50]. Moreover, gamma oscillations in parietal cortex have been found to represent the planned spatial direction for both of saccades [4] and reaching movements [5]. Surface EEG reflects the synchronous activity of large ensembles of rhythmically firing neurons. Such synchronous firing of neurons in the gamma frequency band can serve as a gain control mechanism [51], amplifying the effect of local neuronal firing on downstream areas [48]. For both spatially directed saccades and reaches, amplification of the effects of local neuronal synchronization would increase the effectiveness of transfer of motor planning information between brain areas. In particular, communication between parietal and frontal regions would be especially important for spatially directed movements [52]. Synchronization in the gamma band could thus help mediate spatially directed movements of the eyes and arm through enhanced communication between parietal and frontal brain regions.

We used the common spatial patterns algorithm to extract features for the classification. The CSP algorithm is a spatial filter, which projects multichannel signal onto a direction where the separation between two classes can be maximized by considering their spatial distributions of variances in multichannel electrodes such as the patterns of ERS topology in Fig. 13. In particular, the ERS topologies of the gamma band, c_{1-2}, in Fig. 13 illustrate the power increase over frontal as well as parietal regions, while those of the other bands are mostly over parietal regions. Fig. 14 showed c_{1-2} had a higher number of frontal channels with significant power differences between two tasks, compared to the other IMFs. The increase of gamma activity over frontal sites during movement planning also has been found by Perfetti *et al.* [3]. The gamma band power changes over all EEG channels, including frontal and parietal areas, associated with planning reaches and saccades to two spatial targets, resulted in the higher classification rates than use of the other bands, including use of all bands.

We have investigated the changes of EEG features associated with planning spatially directed movements of the hand and eyes. These features can be used to improve motor imagery BCI systems, which are controlled by imaging movement of right and left hands [53]. Most of the motor imagery BCI systems only rely on movement planning of the hand without spatial direction (left or right) and movement of the eyes. Using the scheme of our experiment, it will be possible to increase the number of controls of the motor imagery BCI system. For example, these can be four different movement imagery tasks for each hand. In our experiment, subjects used their right hand only. For future work, we will look into the EEG features during spatially directed movement planning of the left/right hands and eyes.

V. Conclusion

We have shown that MEMD is a powerful tool for decomposing EEG into intrinsic oscillatory components, and that components in the gamma band contain important features associated with planning spatially directed movements of the hand and eyes. Importantly, this analysis was based on single-trial classification, and the classification accuracy was significantly correlated with eventual movement accuracy—the smaller the reaching errors were, the greater was the separation of movement conditions based on classification of gamma oscillations. The estimation of event-related synchronization over the multichannel EEG showed more dynamic spatial differences in gamma oscillations corresponding to the different conditions than the others, which was consistent with the higher variance of CSP features for gamma oscillation to produce the best classification performance.

Appendix A
Common Spatial Patterns

A single trial data has an $N \times T$ matrix $\overline{\mathbf{X}}$ (N is the number of channels and T the number of samples per channel). The spatial covariance of $\overline{\mathbf{X}}$, which is normalized, can be calculated from

$$\overline{\mathbf{C}} = \frac{\overline{\mathbf{X}}\overline{\mathbf{X}}^T}{tr(\overline{\mathbf{X}}\overline{\mathbf{X}}^T)} \tag{6}$$

where $(\cdot)^T$ is the matrix transpose and $\mathrm{tr}(\mathbf{X})$ is the sum of the diagonal elements of $\mathbf{X}$. The spatial covariance $\overline{\mathbf{C}}_{d\in[a,b]}$ for a task, a or b, is produced by the averaged covariance matrix of the trials. CSP trys to find a matrix $\mathbf{W}$ and diagonal matrices $\mathbf{\Lambda}_a$ and $\mathbf{\Lambda}_b$ ($\mathbf{\Lambda}_a + \mathbf{\Lambda}_b = \mathbf{I}$, the identity matrix) with elements $d \in [\mathrm{a}, \mathrm{b}]$ such that

$$\mathbf{W}^T\overline{\mathbf{C}}_a\mathbf{W} = \mathbf{\Lambda}_a, \quad \mathbf{W}^T\overline{\mathbf{C}}_b\mathbf{W} = \mathbf{\Lambda}_b. \tag{7}$$

The composite spatial covariance is calculated as

$$\mathbf{C}_c = \overline{\mathbf{C}}_a + \overline{\mathbf{C}}_b \tag{8}$$

where $\mathbf{C}_c$ is factored as $\mathbf{C}_c = \mathbf{U}_c\mathbf{\Lambda}_c\mathbf{U}_c^T$, where $\mathbf{U}_c$ is the eigenvector matrix, and $\mathbf{\Lambda}_c$ is the diagonal matrix of eigenvalues. Using the whitening transformation, $\mathbf{P} = \sqrt{\mathbf{\Lambda}_c^{-1}}\mathbf{U}_c^T$, the variances in the space spanned by $\mathbf{U}_c$ are equalized, which makes all the eigenvalues of $\mathbf{P}\mathbf{C}_c\mathbf{P}^T$ equal to unity. Secondly, let $\mathbf{S}_a = \mathbf{P}\overline{\mathbf{C}}_a\mathbf{P}^T$ and $\mathbf{S}_b = \mathbf{P}\overline{\mathbf{C}}_b\mathbf{P}^T$, then $\mathbf{S}_a$ and $\mathbf{S}_b$ share the common eigenvector matrix, that is

$$\mathbf{B}^T\mathbf{S}_a\mathbf{B} = \mathbf{\Lambda}_a, \quad \mathbf{B}^T\mathbf{S}_b\mathbf{B} = \mathbf{\Lambda}_b \quad (\mathbf{\Lambda}_a + \mathbf{\Lambda}_b = \mathbf{I}). \tag{9}$$

The final spatial filter that satisfies (7) is given by $\mathbf{W}^T = \mathbf{B}^T\mathbf{P}$, since we assume the eigenvalues $\mathbf{\Lambda}_a$ are sorted in a descending order. Then the EEG signals can be projected as

$$\mathbf{Z} = \mathbf{W}^T\mathbf{X}. \tag{10}$$

Each column vector $\mathbf{w}_j (j = 1, \ldots, N)$ of $(\mathbf{W}^T)^{-1}$ is a spatial filter, or simply a filter. In order to discriminate between two motor imagery tasks, the variances of the spatially filtered signals using (10) are used as a feature. The row vectors $\mathbf{z}_p (p = 1, \ldots, m$ and $N - m + 1, \ldots, N)$ from $\mathbf{Z}$ that maximize the difference in the variance between the two groups are associated with the largest eigenvalues in $\mathbf{\Lambda}_a$ and $\mathbf{\Lambda}_b$. These signals are contained in the m first and last rows of $\mathbf{Z}$ in (10), due to the calculation of $\mathbf{W}^T$. The interesting features can be calculated as

$$f_p = \mathtt{log}\left(\frac{\mathtt{var}(\mathbf{z}_p)}{\sum_{i=1,\ldots,m \text{ and } N-m+1,\ldots,N}\mathtt{var}(\mathbf{z}_i)}\right) \tag{11}$$

where the symbol $\mathtt{var}(\cdot)$ denotes the variance.

References

[1] O. Bock and R. Eckmiller, "Goal-directed arm movements in absence of visual guidance: Evidence for amplitude rather than position control," *Exp. Brain Res.*, vol. 62, no. 3, pp. 451–458, 1986.

[2] Y. Pertzov, G. Avidan, and E. Zohary, "Multiple reference frames for saccadic planning in the human parietal cortex," *J. Neurosci.*, vol. 31, no. 3, pp. 1059–1068, 2011.

[3] B. Perfetti, C. Moisello, E. C. Landsness, S. Kvint, S. Lanzafame, M. Onofrj, A. D. Rocco, G. Tononi, and M. F. Ghilardi, "Modulation of gamma and theta spectral amplitude and phase synchronization is associated with the development of visuo-motor learning," *J. Neurosci.*, vol. 31, no. 41, pp. 14 810–14 819, 2011.

[4] J. Werf, O. Jensen, P. Fries, and W. P. Medendorp, "Gamma-band activity in human posterior parietal cortex encodes the motor goal during delayed prosaccades and antisaccades," *J. Neurosci.*, vol. 28, no. 34, pp. 8397–8405, 2008.

[5] J. V. D. Werf, O. Jensen, P. Fries, and W. P. Medendorp, "Neuronal synchronization in human posterior parietal cortex during reach planning," *J. Neurosci.*, vol. 30, no. 4, pp. 1402–1412, 2010.

[6] C. S. Herrmann, I. Fründ, and D. Lenz, "Human gamma-band activity: A review on cognitive and behavioral correlates and network models," *Neurosci. Biobehav. Rev.*, vol. 34, no. 7, pp. 981–992, 2010.

[7] N. E. Huang, Z. Shen, S. R. Long, M. L. Wu, H. H. Shih, Z. Quanan, N. C. Yen, C. C. Tung, and H. H. Liu, "The empirical mode decomposition and the Hilbert spectrum for nonlinear and non-stationary time series analysis," in *Proc. R. Soc. A*, 1998, vol. 454, no. 1971, pp. 903–995.

[8] C. Park, D. Looney, N. Rehman, A. Ahrabian, and D. P. Mandic, "Classification of motor imagery BCI using multivariate empirical mode decomposition," *IEEE Trans. Neural Syst. Rehabil. Eng.*, vol. 21, no. 1, pp. 10–22, Jan. 2013.

[9] D. Looney, L. Li, T. Rutkowski, D. P. Mandic, and A. Cichocki, "Ocular artifacts removal from EEG using EMD," in *Proc. 1st Int. Conf. Cognitive Neurodynam.*, 2007, pp. 831–835.

[10] C. Park, D. Looney, P. Kidmose, M. Ungstrup, and D. P. Mandic, "Time-frequency analysis of EEG asymmetry using bivariate empirical mode decomposition," *IEEE Trans. Neural Syst. Rehabil. Eng.*, vol. 19, no. 4, pp. 366–373, Aug. 2011.

[11] H. Liang, S. L. Bressler, E. A. Buffalo, R. Desimone, and P. Fries, "Empirical mode decomposition of field potentials from macaque V4 in visual spatial attention," *Biol. Cybern.*, vol. 92, no. 6, pp. 380–392, 2005.

[12] C. M. Sweeney-Reed and S. J. Nasuto, "A novel approach to the detection of synchronisation in EEG based on empirical mode decomposition," *J. Computat. Neurosci.*, vol. 23, no. 1, pp. 79–111, 2007.

[13] T. Rutkowski, D. P. Mandic, A. Cichocki, and A. Przybyszewski, "EMD approach to multichannel EEG data analysis—The amplitude and phase components clustering analysis," *J. Circuits, Syst. Comput.*, vol. 19, no. 1, pp. 215–229, 2010.

[14] D. Looney and D. P. Mandic, "Multi-scale image fusion using complex extensions of EMD," *IEEE Trans. Signal Process.*, vol. 57, no. 4, pp. 1626–1630, Apr. 2009.

[15] N. Rehman and D. P. Mandic, "Multivariate empirical mode decomposition," in *Proc. R. Soc. A*, 2010, vol. 466, no. 2117, pp. 1291–1302.

[16] B. Bathellier, L. Ushakova, and S. Rumpel, "Discrete neocortical dynamics predict behavioral categorization of sounds," *Neuron*, vol. 76, no. 2, pp. 435–449, 2012.

[17] Y. Wang and T. P. Jung, "A collaborative brain-computer interface for improving human performance," *PLoS ONE*, vol. 6, no. 5, pp. 1–11, 2011.

[18] H. Drucker, C. J. C. Burges, L. Kaufman, A. J. Smola, and V. Vapnik, , M. C. Mozer, M. I. Jordan, and T. Petsche, Eds*., Support Vector Regression Machines*. Cambridge, MA: MIT Press, 1997.

[19] G. Rilling, P. Flandrin, and P. Gonçalves, "On empirical mode decomposition and its algorithms," in *Proc. IEEE-EURASIP Workshop NSIP*, 2003, vol. 3, pp. 8–11.

[20] L. Cohen, "Instantaneous anything," in *Proc. IEEE Int. Conf. Acoust., Speech Signal Process.*, 1993, vol. 5, pp. 105–108.

[21] J. Cui and W. Freeden, "Equidistribution on the sphere," *J. Sci. Comput.*, vol. 18, no. 2, pp. 595–609, 1997.

[22] N. E. Huang, M. L. Wu, S. R. Long, S. S. P. Shen, W. Qu, P. Gloersen, and K. L. Fan, "A confidence limit for the empirical mode decomposition and Hilbert spectral analysis," in *Proc. R. Soc. A*, 2003, vol. 459, no. 2037, pp. 2317–2345.

[23] N. Rehman and D. P. Mandic, "Filter bank property of multivariate empirical mode decomposition," *IEEE Trans. Signal Process.*, vol. 59, no. 5, pp. 2421–2426, May 2011.

[24] J. Snider, M. Plank, D. Lee, and H. Poizner, "Simultaneous neural and movement recording in large-scale immersive virtual environments," *IEEE Trans. Biomed. Circuits Syst.*, vol. 7, no. 5, pp. 713–721, Oct. 2013.

[25] J. Trommershäuser, L. T. Maloney, and M. S. Landy, "Statistical decision theory and the selection of rapid, goal-directed movements," *J. Opt. Soc. A*, vol. 20, no. 7, pp. 1419–1433, 2003.

[26] S. Gepshtein, A. Seydell, and J. Trommershäuser, "Optimality of human movement under natural variations of visual-motor uncertainty," *J. Vis.*, vol. 7, no. 5, pp. 1–18, 2007.

[27] S. Gepshtein, X. Li, J. Snider, M. Plank, D. Lee, and H. Poizner, "Dopamine function and the efficiency of human movement," *J. Cognitive Neurosci.*, vol. 26, no. 3, 2014.

[28] A. Delorme and S. Makeig, "EEGLAB: An open source toolbox for analysis of single-trial EEG dynamics including independent component analysis," *J. Neurosci. Methods*, vol. 134, no. 1, pp. 9–21, 2004.

[29] S. Makeig, A. J. Bell, T. P. Jung, and T. J. Sejnowski, , D. Touretzky, M. Mozer, and M. Hasselmo, Eds*., Independent Component Analysis of Electroencephalographic Data*. Cambridge, MA: MIT Press, 1996, vol. 8, Adv. Neural Inf. Process. Syst..

[30] B. Perfetti, C. Moisello, E. Landsness, S. Kvint, A. Pruski, M. Onofrj, G. Tononi, and M. Ghilardi, "Temporal evolution of oscillatory activity predicts performance in a choice-reaction time reaching task," *J. Neurophysiol.*, vol. 105, no. 1, pp. 18–27, 2011.

[31] A. Bell and T. Sejnowski, "An information-maximization approach to blind separation and blind deconvolution," *Neural Computat.*, vol. 7, no. 6, pp. 1129–1150, 1995.

[32] T. Jung, S. Makeig, M. Westerfield, J. Townsend, E. Courchesne, and T. Sejnowski, "Removal of eye activity artifacts from visual event-related potentials in normal and clinical subjects," *Clin. Neurophysiol.*, vol. 111, no. 10, pp. 1745–1758, 2000.

[33] J. T. Gwin, K. Gramann, S. Makeig, and D. P. Ferris, "Removal of movement artifact from high-density EEG recorded during walking and running," *J. Neurophysiol.*, vol. 103, pp. 3526–3534, 2010.

[34] P. Lee, J. Sie, Y. Liu, C. Wu, M. Lee, C. Shu, P. Li, C. Sun, and K. Shyu, "An SSVEP-actuated brain computer interface using phase-tagged flickering sequences: A cursor system," *Ann. Biomed. Eng.*, vol. 38, no. 7, pp. 2383–2397, 2010.

[35] S. Hadjidimitriou, P. Doulgeris, and L. Hadjileontiadis, "Revealing action representation processes in audio perception using fractal EEG analysis," *IEEE Trans. Biomed. Eng.*, vol. 58, no. 4, pp. 1120–1129, Apr. 2011.

[36] H. Ramoser, J. Müller-Gerking, and G. Pfurtscheller, "Optimal spatial filtering of single trial EEG during imagined hand movement," *IEEE Trans. Rehabil. Eng.*, vol. 8, no. 4, pp. 441–446, Dec. 2000.

[37] J. Müller-Gerking, G. Pfurtscheller, and H. Flyvbjerg, "Designing optimal spatial filters for single-trial EEG classification in a movement task," *Clin. Neurophysiol.*, vol. 110, no. 5, pp. 787–798, 1999.

[38] S. S. Keerthi and C. Lin, "Asymptotic behaviors of support vector machines with gaussian kernel," *Neural Computat.*, vol. 15, no. 7, pp. 1667–1689, 2003.

[39] C. C. Chang and C. J. Lin, "LIBSVM: A library for support vector machines," *ACM Trans. Intell. Syst. Technol.*, vol. 2, no. 3, pp. 1–27, 2011.

[40] J. Kalcher and G. Pfurtscheller, "Discrimination between phase-locked and non-phase-locked event-related EEG activity," *Electroencephalogr. Clin. Neurophysiol.*, vol. 94, no. 5, pp. 381–384, 1995.

[41] P. Stoica and R. L. Moses*, Introduction to Spectral Analysis*. Upper Saddle River, NJ: Prentice Hall, 1997, vol. 1.

[42] G. Pfurtscheller, C. Neuper, C. Brunner, and F. L. Silva, "Beta rebound after different types of motor imagery in man," *Neurosci. Lett.*, vol. 378, no. 3, pp. 156–159, 2005.

[43] J. A. Hanley and B. J. McNeil, "A method of comparing the areas under receiver operating characteristic curves derived from the same cases," *Radiology*, vol. 148, no. 3, pp. 839–843, 1983.

[44] J. Sørensen, L. Johannesen, U. Grove, K. Lundhus, J. Couderc, and C. Graff, "A comparison of IIR and wavelet filtering for noise reduction of the ECG," *Comput. Cardiol.*, vol. 37, pp. 489–492, 2010.

[45] M. Plank, S. Hillyard, C. Huang, D. Alonzo, S. Gepshtein, and H. Poizner, "Eye-hand coordination and EEG microstates associated with rapid pointing under risk and uncertainty," presented at the Cognitive Neurosci. Soc. Annu. Meet., San Francisco, CA, 2011.

[46] D. Lenz, K. Krauel, J. Schadow, L. Baving, E. Duzel, and C. S. Herrmann, "Enhanced gamma-band activity in ADHD patients lacks correlation with memory performance found in healthy children," *Brain Res.*, vol. 1235, pp. 117–132, 2008.

[47] T. J. Sejnowski and O. Paulsen, "Network oscillations: Emerging computational principles," *J. Neurosci.*, vol. 26, no. 6, pp. 1673–1676, 2006.

[48] J. L. O. Jensen and J. Kaiser, "Human gamma-frequency oscillations associated with attention and memory," *Trends Neurosci.*, vol. 30, no. 7, pp. 317–324, 2007.

[49] R. A. Joundi, N. Jenkinson, J. Brittain, T. Z. Aziz, and P. Brown, "Driving oscillatory activity in the human cortex enhances motor performance," *Curr. Biol.*, vol. 22, no. 5, pp. 403–407, 2012.

[50] N. Jenkinson, A. Kühn, and P. Brown, "Gamma oscillations in the human basal ganglia," *Exp, Neurol,*, vol. 245, pp. 72–76, 2013.

[51] S. Emilio and T. J. Sejnowski, "Correlated neuronal activity and the flow of neural information," *Nat. Rev.*, vol. 2, pp. 539–550, 2001.

[52] J. Gallivan, D. McLean, F. Smith, and J. Culham, "Decoding effector-dependent and effector-independent movement intentions from human parieto-frontal brain activity," *J. Neurosci.*, vol. 31, no. 47, pp. 17 149–17 168, 2011.

[53] G. Pfurtscheller, C. Neuper, D. Flotzinger, and M. Pregenzer, "EEG-based discrimination between imagination of right and left hand movement.," *Electroencephalogr. Clin. Neurophysiol.*, vol. 103, no. 6, pp. 642–651, 1997.

Cheolsoo Park received the B.Eng. degree in electrical engineering from Sogang University, Seoul, South Korea, the M.Sc. degree in biomedical engineering department from Seoul National University, Seoul, South Korea, and the Ph.D. degree in adaptive nonlinear signal processing from Imperial College London, London, U.K., in 2012.

He worked as a postdoctoral researcher in Bioengineering Department at the University California-San Diego, La Jolla, CA, USA, in 2012. Currently he is an Assistant Professor at Kwangwoon University, Seoul, Korea. His research interests are mainly in the area of machine learning, adaptive and statistical signal processing, with applications in brain–computer interface and computational neuroscience.

Markus Plank received the doctorate degree at the Ludwig-Maximilians-University of Munich, Munich, Germany, where he investigated the EEG correlates of internal reference frames during spatial navigation.

He is a Scientific Consultant at Brain Products GmbH, Gilching, Germany. His primary interest is in innovative methodological and computational approaches to mobile brain imaging. During his postdoctoral research at the Poizner Lab (University California-San Deigo, La Jolla, CA, USA) his work focused primarily on the neurophysiological basics of spatial learning and memory in virtual reality utilizing independent component analysis, source reconstruction of electrical dipoles, and time-frequency decomposition of high-density EEG arrays.

Joseph Snider is a Research Scientist in the Institute of Neural Computation, at the University California-San Deigo, La Jolla, CA, USA. He is trained as a computational physicist and now applies computational and theoretical techniques to the large scale data sets created by the combination of neural and movement recordings.

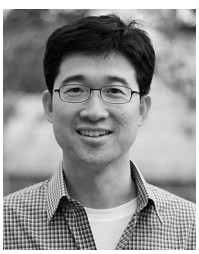

Sanggyun Kim (S'02–M'09) received the Ph.D. degree in electrical engineering and computer science from the Korea Advanced Institute of Science and Technology, Daejeon, Korea, in 2008.

He joined the Statistical Learning for Signal Processing Laboratory, School of Electrical Engineering and Computer Science at Korea Advanced Institute of Science and Technology, Daejeon, Korea, in 2001. He was a postdoctoral researcher at the Department of Brain and Cognitive Sciences, Massachusetts Institute of Technology, Cambridge, MA, USA, from January 2009 to June 2010, and in Coordinated Science Lab at University of Illinois Urbana and Champaign, Champaign, IL, USA, from July 2010 to June 2011. He is currently an Assistant Project Scientist in Bioengineering at the University of California-San Diego, La Jolla, CA, USA. His research interests include statistical signal processing, machine learning and information theory with applications to neuroscience and multimedia data.

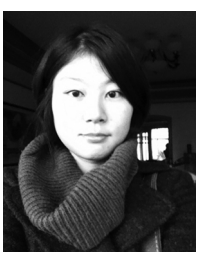

He Crane Huang is currently a Ph.D. degree candidate in cognitive science at the University of California-San Diego, La Jolla, CA, USA.

She is interested in using computational models (Bayesian models and optimal control theory) to understand sensory-motor processing in human behavior.

Sergei Gepshtein is a scientist at the Center for Neurobiology of Vision at the Salk Institute for Biological Studies, La Jolla, CA, USA. Trained in neurobiology (Weizmann Institute of Science), psychology (University of Virginia), and vision science (University of California, Berkeley), he was a member of the Computational Neuroscience Group at RIKEN Brain Science Institute, Japan, before he joined the Salk Institute in 2007. His research concerns foundations of sensory neuroscience, focusing on the normative models of visual perception, inter-sensory integration, and sensorimotor control.

Mr. Gepshtein is a recipient of the inaugural Hay Grant Award (2013) from the Academy of Neuroscience for Architecture.

Todd P. Coleman (S'01–M'05–SM'11) received the Ph.D. degree in electrical engineering from the Massachusetts Institute of Technology, Cambridge, MA, USA, in 2005.

He was a postdoctoral scholar in neuroscience at the Massachusetts Institute of Technology and Massachusetts General Hospital during the 2005–2006 academic year. He was an Assistant Professor in Electrical and Computer Engineering and Neuroscience at the University of Illinois from 2006 to 2011. He is currently an Associate Professor in Bioengineering and director of the Neural Interaction Laboratory at the University of California-San Diego, La Jolla, CA, USA. His research is highly interdisciplinary and lies at the intersection of bio-electronics, neuroscience, medicine, and applied mathematics.

Dr. Coleman is a science advisor for the Science & Entertainment Exchange (National Academy of Sciences).

Howard Poizner is a Research Scientist in the Institute of Neural Computation at the University of California-San Diego (UCSD), La Jolla, CA, USA and Professor Emeritus of Neuroscience at Rutgers University, New Brunswick, NJ, USA. He was a postdoc, staff scientist, and Associate Director of the Laboratory for Cognitive Neuroscience at the Salk Institute for Biological Studies from 1978 to 1989. From 1989 to 2004 he was a Professor and then Distinguished Professor of Neuroscience at Rutgers University. He came to UCSD in 2005. His research interests involve unsupervised learning, the neural control of movement and the integration of brain and movement recordings in virtual environments.